ChemComm

Shape-Controlled Synthesis of Mesoporous Iron Phosphate with Crystallized Frameworks

Journal:	*ChemComm*
Manuscript ID:	CC-COM-05-2015-004356.R1
Article Type:	Communication
Date Submitted by the Author:	28-Jun-2015
Complete List of Authors:	Malay, Pramanik; National Institute for Materials Science, Imura, Masataka; National Institute for Materials Science, WPI Center for MANA Lin, Jianjian; University of Wollongong, Institute for Superconducting and Electronics Materials Kim, Jung Ho; University of Wollongong, Kim, Jung Ho; Institute for Superconducting and Electronic Materials, Yamauchi, Yusuke; National Institute for Materials Science, WPI Center for MANA

Journal Name

COMMUNICATION

Shape-Controlled Synthesis of Mesoporous Iron Phosphate with Crystallized Frameworks

Received 00th January 20xx,
Accepted 00th January 20xx

DOI: 10.1039/x0xx00000x

www.rsc.org/

Malay Pramanik[a], Masataka Imura[a], Jianjian Lin[b], Jeonghun Kim[b], Jung Ho Kim[b*], and Yusuke Yamauchi[a,c*]

Herein, we report the preperation of crystalline mesoporous iron phosphate ($FePO_4$, hereafter abbreviated as FeP) materials with 2D-plates and 1D-rods in presence of an amphiphilic block copolymer (F127), iron nitrate, and phosphoric acid. The dimensanility of mesoporous FeP can be switched by changing the polarity of the synthetic medium.

Synthesis of mesostructured materials with well-defined morphology for various transition metal oxides, chalcogenides, and phosphates is of pronounced research interest due to their great potential applications in electrochemical energy storage devices, such as fuel cells, supercapacitors, and Li-ion batteries.[1-4] For example, various oxides with rod/tube-like morphology and iron based phosphates with plate-like morphology have shown superior efficiency over bulk material as an electrode in rechargeable batteries.[5-6] Therefore, controlled synthesis of different shaped materials is very crucial for development of the next generation of batteries. In spite of a great deal of interest, the synthesis of mesoporous transition-metal-based materials, particularly phosphate materials, has encountered many hurdles as a result of problems in controlling hydrolysis and condensation, due to the high reactivity of the metal precursors.[7,8] Several efforts have been made to date to solve the above problems.[9,10] An effective strategy for controlling the reactions of transition metals was proposed that involves using additives as stabilizing agents.[11] The use of non-aqueous solvents is also effective for decreasing the reactivity of metal precursors.[12,13] Another strategy is the formation of mesostructured materials from very dilute initial concentrations of metal ions through the evaporation-induced-self-assembly (EISA) method.[14] The aim of all the above procedures is to delay the rapid condensation reactions of the inorganic precursors, which lead to the formation of bulk materials and uncontrolled phase separation between the organic and inorganic components. Although there are a few published reports on the successful synthesis of mesoporous transition-metal-based oxide and chalcogenide materials with controlled shapes,[3,15-17] there have been no reports on transition-metal-based phosphate materials due to the rapid condensation reaction of the precursors.[18] Therefore, a precise pathway for synthesis of mesoporous phosphate materials with well-controlled shapes is still required for further materials synthesis and engineering.

Non-siliceous mesoporous inorganic solids, especially mesoporous metallophosphates (Sn, Ni, Ti, Fe, and V) have attracted a great deal of interest over the decades due to their potential applications in catalysis, adsorption, separation, and electronics.[19,20] Mesoporous iron phosphates in particular have attracted immense interest for both conventional chemical research and emerging applications in portable electronic devices and Li-ion batteries.[21-24] Controlling the morphology and mesoporous architecture of mesoporous iron phosphate is very crucial to obtain the superior electrochemical properties that are needed for an energy storage material.[24] Simultaneous control over both the morphology and the porous nanostructure still remain a challenging problem, however, especially for materials with complex crystal structures (e.g., iron phosphate) due to the rapid hydrolysis of the inorganic Fe-precursor in the aqueous phosphonic acid medium.[24,25] Mesostructured iron phosphate materials have been reported based on the self-organization of low-molecular-weight ionic surfactants (e.g., cetyl trimethyl ammonium bromide (CTAB), sodium dodecyl sulfate (SDS) in aqueous medium.[24,26,27] The pore walls are amorphous, however. Because the ionic structure directing agents (SDAs) for the self-assembly show poor structural stability in an aqueous medium, novel morphologies with mesoporous structure are hard to achieve.[28] In contrast, non-ionic block copolymers are a fascinating class of SDAs due to their variety of self- assembly characteristics.[27] Thus, the morphologies can be tuned by adjusting the solvent compositions, molecular weights, and polymer blocks.[29]

Here, we have for the first time prepared new crystalline mesoporous iron phosphate materials (FeP) with different shapes in the presence of a commercially available non-ionic amphiphilic triblock copolymer, Pluronic F127, as a structure directing agent in a non-aqueous medium. The size and the morphology of the mesostructured iron phosphate are controlled by adjusting the solvent composition in the synthetic medium. Two-dimensional (2D) plates and one-dimensional (1D) rods have been successfully

[a] *International Center for Materials Nanoarchitectonics (MANA), National Institute for Materials Science (NIMS), 1-1 Namiki, Tsukuba, Ibaraki 305-0044 (Japan).*
[b] *Institute for Superconducting and Electronic Materials (ISEM), University of Wollongong (UOW), Innovation Campus, North Wollongong, NSW 2500 (Australia).*
[c] *Department of Nanoscience and Nanoengineering, Faculty of Science and Engineering, Waseda University, 3-4-1 Okubo, Shinjuku, Tokyo 169-8555 (Japan).*
† Electronic Supplementary Information (ESI) available: [details experimental procedures, elemental mapping, XRD, SEM, XPS, morphology switching and electrochemical data. See DOI: 10.1039/x0xx00000x

synthesized in a selective way. In the case of acidic ethanol as the synthetic medium, very uniform mesostructured FeP 2D plates are formed. In case of acidic tetrahydrofuran (THF) as the synthetic medium, mesostructured FeP 1D rods are formed. The parent mesostructures and morphologies are retained, even after the crystallization of the pore walls by calcination. This simple and unique method will be widely applicable to control the morphology/dimensionality of other transition-metal-based phosphate materials in the future (experimental section, ESI†).

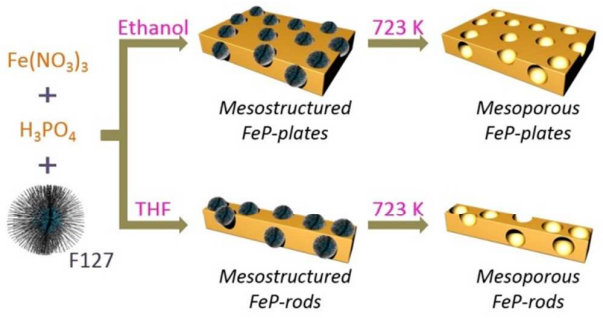

Scheme 1 Schematic illustration of the formation of mesoporous FeP plates and FeP rods with crystalline pore walls.

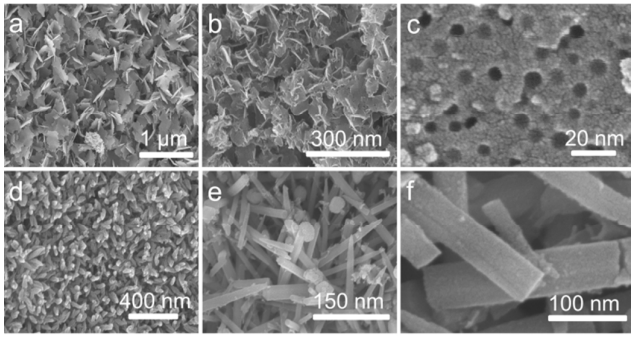

Fig. 1 SEM images of (a) mesostructured FeP plates before calcination, (b, c) mesoporous FeP plates after calcination, (d) mesostructured FeP rods before calcination and (e, f) mesoporous FeP rods after calcination.

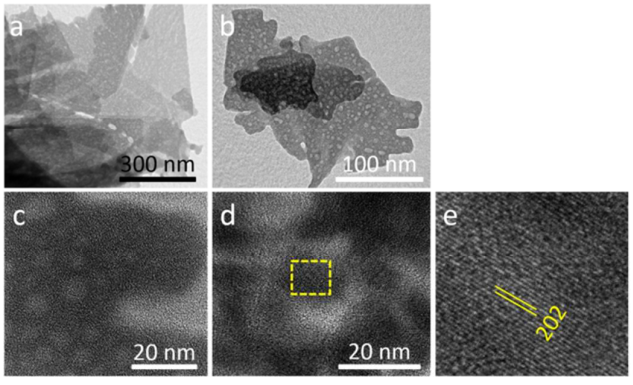

Fig. 2 TEM images of (a) mesostructured FeP plates before calcination, (b-e) mesoporous FeP plates after calcination.

Here, we have prepared two crystalline mesoporous FeP materials, with two different morphologies, by varying the solvents of the synthetic medium (Scheme 1). Fig. 1 shows scanning electron microscope (SEM) images of the as-prepared mesostructured FeP and calcined mesoporous FeP materials. Fig. 1a shows the 2D plate-like morphology of the as-synthesized FeP obtained from ethanol medium. The width of the flakes is measured to be around 20 nm (Fig. 1a). Even after calcination, the original flake-like morphology is completely retained (Fig. 1b), although the lateral size is slightly reduced. The templates are successfully removed by the calcination. Uniformly sized mesopores are observable on the surfaces of the plates (Fig. 1c). The pore diameters are measured to be around 6 nm. Fig. 1d shows the 1D rod-like morphology of the as-prepared FeP obtained from THF medium. Even though the diameters of the rods are slightly decreased from 34 nm to 22 nm (average sizes) by the calcination, the 1D rod-like morphology is mostly retained (Fig. 1e-f). The mesoporous structures were also carefully observed by transmission electron microscopy (TEM). After calcination, the organic templates are removed completely to form mesopores around 6 nm in diameter on average (Fig. 2 and 3). As control experiments, various FeP materials were prepared in mixed solvents (*i.e.*, EtOH:H_2O (1:1) and THF:H_2O (1:1)) and different polar solvents (*i.e.*, water, acetonitrile, methanol, and propanol). The corresponding SEM images of the as-prepared FeP materials are shown in Fig S1, ESI†.

Low-angle X-ray diffraction (XRD) patterns of the mesoporous FeP plates and rods are shown in Fig. 4a. The two materials show a distinctive intense broad peak centered at 2θ = 1.04° and 1.15°, respectively, for the mesoporous plates and rods, with no higher order peaks, which corresponds to the characteristic of a less-ordered/disordered mesoporous structure.[31] The *d*-spacing corresponds to around 8.5 and 7.7 nm for the mesoporous plates and rods, respectively. These values are attributable to the average pore-to-pore distance (equal to the total values of the pore sizes and pore walls). The mesoporous structures in the materials are generated due to the cooperative self-assembly of Pluronic F127 and inorganic species in the synthetic medium.[32] The elemental analysis for both samples proves the presence of iron, phosphorus, and oxygen over the entire area (Fig. S2, ESI†). The wide angle XRD patterns of the as-prepared FeP plates and rods before the calcination show no obvious peaks, meaning that the pore walls are amorphous (Fig. S3, ESI†). The pore walls are crystallized by the calcination. Wide-angle XRD patterns of the calcined mesoporous FeP plates and rods are shown in Fig. 4b. For the two materials, the peak positions are exactly the same, although the obtained wide-angle XRD patterns do not match any standard JCPDS cards. Therefore, to obtain the details of the crystal structure, Rietveld refinement was carried out by employing the MAUD program.[33]

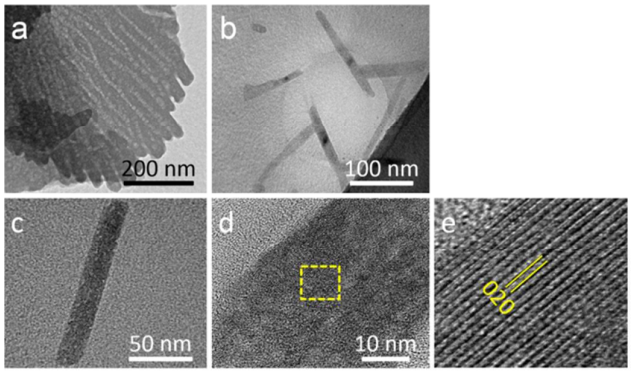

Fig. 3 TEM images of (a) mesostructured FeP rods before calcination, (b-e) mesoporous FeP rods after calcination.

After the final refinement, the crystal structure of the materials was assigned to the monoclinic crystal structure with unit cell

parameters a = 15.715(7) Å, b = 11.505(3) Å, c = 6.736(2) Å, and β = 92.503(3)°. The experimental and simulated XRD patterns are shown in Fig. 4b, and the model for the FeP crystal structure is shown in Fig. 4c. From the high resolution TEM images, crystal fringes are clearly observed inside the pore walls (Fig. 2e and 3e). In the case of the mesoporous FeP plates, the distance between the observed two fringes (indicated by the solid line in Fig. 2e) are in good agreement with the (202) crystal planes of the monoclinic crystal structure. In the case of the mesoporous FeP rods, the crystal fringes are coherently oriented along the long axis of the rod. The distance between two consecutive crystal fringes (Fig. 3e) is in good agreement with the (020) crystal planes of the monoclinic crystal structure. The average crystallite sizes of FeP-plates and FeP-rods were calculated by the Sherrer equation (D = 0.9λ/βcosθ). The average crystalline sizes are *ca.* 53 and 64 nm for FeP-plates and FeP-rods respectively. These sizes are much larger than the average pore-to-pore distance obtained in Fig. 4a. Therefore, the crystal fringes are coherently extended across several mesopores, as shown in Figs. 2 and 3.

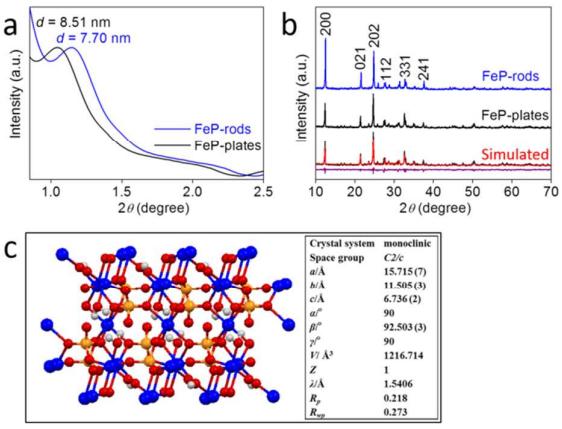

Fig. 4 (a) Low-angle XRD patterns of mesoporous FeP rods and plates after calcination. (b) Wide-angle XRD patterns of mesoporous FeP rods and plates after calcination, computed XRD pattern for the FeP plates, and the difference between the experimental and the computed XRD patterns. (c) Model of the crystal structure of FeP with detailed crystal parameters.

Although in the wide-angle XRD patterns, the peak positions of the two materials remain exactly same, the intensities of the two major peak at 2θ = 12.50° and 24.80° vary hugely (Fig. 4b). The peaks at 2θ = 12.50° and 24.80°reflect the (200) and (202) crystal plane of the materials. In case of the mesoporous rods, the intensity of the (200) diffraction peak is stronger than for any other peaks, which indicates crystal growth along the a-axis, leading to the formation of highly crystallized rods, which is in good agreement with the TEM data (Fig. 3e). In contrast, in the case of the mesoporous plates, the intensity of the (202) diffraction peak is stronger than for any other peaks, which indicates the favorable 2D growth of the crystallized plates along the a and c-axes (Fig. 2e).

The chemical composition and local structure of FeP materials was investigated by X-ray photoelectron spectroscopy (XPS) also (Fig. S4, ESI†). From the XPS survey spectrum, the elemental composition (Fe/P/O) was calculated to be 1.0/0.9/4.3, respectively. The value for Fe/P (1.0/ 0.9) is almost the same as the initial reaction composition of 1/1. From high resolution XPS spectra, the peak positions of Fe 2$p_{3/2}$, Fe 2$p_{1/2}$, P 2$p_{3/2}$, and O 1*s* are in good agreement with the previously reported FeP material.[34] The porosity of the materials was investigated by N_2 adsorption-desorption isotherms at liquid N_2 temperature (Fig. 5). The isotherms of the materials can be classified as type IV isotherms with hysteresis loops (Fig. 5a).[35] The large hysteresis loops, particularly for the mesoporous plates, in the P/P_0 range of 0.60 to 0.95 indicate that large-sized cage-like mesopores are connected each other through small size windows.[36] The corresponding pore size distribution curves were obtained by BJH method (Fig. 5b). After calcination at 723 K, the material produces uniform mesopores around 5.8 nm in diameter. This size corresponds to the SEM and TEM data, as shown in Fig. 1c, 2c, and 3d. This pore size is quite similar to those of other mesoporous materials prepared using Pluronic F127 as a template.[31] Even though the solvents are different, the diameter of the mesopores remains constant. The corresponding Brunauer-Emmett-Teller (BET) surface areas and pore volumes are 295 $m^2 \cdot g^{-1}$ and 0.31 $cm^3 \cdot g^{-1}$ (for mesoporous FeP plates), and 272 $m^2 \cdot g^{-1}$ and 0.27 $cm^3 \cdot g^{-1}$ (for mesoporous FeP rods), respectively.

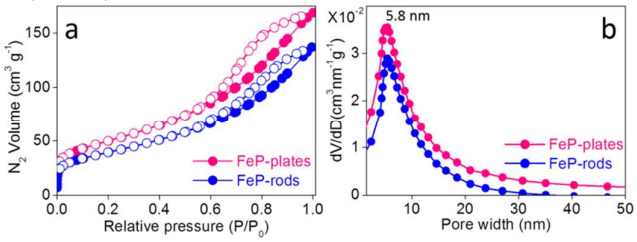

Fig. 5 (a) N2 adsorption-desorption isotherms of mesoporous FeP plates and FeP rods. (b) Pore size distribution curves of mesoporous FeP plates and FeP rods.

Such crystalline FeP materials with high surface area, unique morphology, and large, uniform mesopores have been never reported. Although there are a few reports of mesoporous FeP materials, the pore walls are basically amorphous, and the materials have small-sized mesopores (less than 3 nm) with low surface area (less than 150 $m^2 \cdot g^{-1}$).[24,26] As mentioned above, the *d*-spacing corresponds to around 8.5 and 7.7 nm for the mesoporous plates and rods, respectively. These values are attributable to the average pore-to-pore distance. Considering the pore size obtained by the BJH method, the pore walls in the mesoporous rods, are slightly thinner compared to the mesoporous plates. As shown in Fig. 3d, the mesopores are more densely packed inside the rods.

In general, 'rapid crystallization' produces fine nanoparticles with irregular sizes, while 'slow crystallization' can allow for the production of well-defined macroscopic morphology similar to the inherent atomic crystal structure.[37] In our present synthesis, we have also prepared mesostructured FeP materials with well-defined morphology by very slow crystallization in a non-aqueous medium. As mentioned above, the as-prepared materials do not have any wide-angle X-ray diffraction peaks, indicating that the pore walls are amorphous and/or poorly crystalized (Fig. S3, ESI†). Therefore, in our present synthetic procedure, the 1D/2D macroscopic morphologies of the materials are not controlled by their inherent atomic crystal structure like 1D ZnSe, or 2D MoS_2, or graphene sheets.[38,39]

To study the formation mechanism of our mesostructured FeP plates and FeP rods, the formation of FeP materials was carried out in the absence of F127 in the ethanol and THF media, respectively. The as-prepared FeP materials do not show any plate- or rod-like morphologies (Fig. S5a-b, ESI†). Therefore, it is expected that the

mesostructured FeP plates or FeP rods are likely to have evolved from the cooperative assembly of spherical micelles composed of F127 and inorganic species ($Fe(NO_3)_3$ and H_3PO_4).[40] The spherical micelles, in which the polypropylene oxide (PPO) domain is core and the polyethylene oxide (PEO) domain is shell, are capable of H-bonding through the -PEO and -PO_4 units.[41] In the case of THF medium, the dielectric constant and H-bonding capability are lower compared to the ethanol medium.[42] Hence, the linear assembly of individual micelles is feasible to decrease the total energy of the system. The similar linear assembly of nanoparticles has, in fact, been observed to minimize the energy of the system.[43,44] We also carried out another reaction in a mixed solvent (with a 1/1 volume ratio of ethanol/THF). In this case, the length of the rods was decreased, and the width slightly increased (Fig. S5c-d, ESI†). The relationship between the length ratios and the solvent compositions is shown in Fig. S6, ESI†. From this observation, it is found that the solvent polarity plays the crucial role in determining the final morphology. Due to the higher H-bonding capability and dielectric constant of ethanol, along with the 1D arrangement of spherical micelles, the effective lateral interaction between the spherical micelles produces 2D plate-like morphology. This phenomenon is correlated with the 2D arrangements of nanoparticles through effective H-bonding by proper surface functionalization.[45,46] We have extended our concept for the synthesis of mesoporous nickel phosphate (NiP) with plates- and rod-like morphology in EtOH and THF medium (Fig. S7, ESI†).

A new set of mesoporous FeP materials with controlled shapes were synthesized in the presence of an amphiphilic triblock copolymer (F127), iron nitrate, and phosphoric acid. By proper selection of solvents, the morphologies of mesoporous FeP materials (i.e. plates and rods) can be easily controlled. To the best of our knowledge, this is the first report on the dimensionally controlled synthesis of mesoporous crystalline FeP materials. We strongly believe that, the simplicity of this synthetic concept will allow us to generalize our method to various other 2D/1D mesoporous crystalline phosphate materials, which will be definitely important for the development for various electrochemical energy storage devices (Fig. S8, ESI†).

Notes and references

1 S. Y. Choi, M. Mamak, N. Coombs, N. Chopra and G. A. Ozin, *Adv. Funct. Mater.*, 2004, **14**, 335.
2 Y. Yu, S. Hou, M. Meng, X. Tao, W. Liu, Y. Lai and B. Zhang, *J. Mater. Chem.*, 2011, **21**, 10525.
3 C. Liu, F. Li, L. P. Ma and H. M. Cheng, *Adv. Mater.*, 2010, **22**, 28.
4 Y. Tang, D. Wu, Y. Mai, H. Pan, J. Cao, C. Yang, F. Zhang and X. Feng, *Nanoscale*, 2014, **6**, 14679.
5 F. Cheng, Z. Tao, J. Liang and J. Chen, *Chem. Mater.*, 2008, **20**, 667.
6 B. L. Ellis, W. R. M. Makahnouk, Y. Makimura, K. Toghill, and L. F. Nazar, *Nat.Mater.*, 2007, **6**, 749.
7 D. Gu and F. Schuth, *Chem. Soc. Rev.*, 2014, **43**, 313.
8 M. Vasylyev and R. Neumann, *Chem. Mater.*, 2006, **18**, 2781.
9 J. Hu, T. W. Odom and C. M. Lieber, *Acc. Chem. Res.*, 1999, **32**, 435.
10 F. Cheng, J. Zhao, W. Song, C. Li, H. Ma, J. Chen and P. Shen, *Inorg. Chem.*, 2006, **45**, 2038.
11 G. J. A. A. Soler-lllia, C. Sanchez, B. Lebeau and J. Patarin, *Chem. Rev.*, 2002, **102**, 4093.
12 S. A. Bagshaw and T. J. Pinnavaia, *Angew Chem. Int. Ed. Engl.*, 1996, **35**, 1102.
13 P. Yang, D. Zhao, B. F. Chmelka, D. I. Margolese and G. D. Stucky, *Chem. Mater.*, 1999, **11**, 2813.
14 C. J. Brinker, Y. Lu, A. Sellinger and H. Fan, *Adv. Mater.*, 1999, **11**, 579.
15 J. S. Hu, L. S. Zhong, W. G. Song and L. J. Wan, *Adv. Mater.*, 2008, **20**, 2977.
16 J. H. Han, S. Lee and J. Cheon, *Chem. Soc. Rev.*, 2013, **42**, 2581.
17 M. B. Zakaria, M. Hu, R. R. Salunkhe, M. Pramanik, K. Takai, V. Malgras, S. Choi, S. X. Dou, J. H. Kim, M. Imura, S. Ishihara and Y. Yamauchi, *Chem. Eur. J.*, 2015, **21**, 3605.
18 R. K. Mah, M. W. Lui and G. K. H. Shimizu, *Inorg. Chem.*, 2013, **52**, 7311.
19 A. Bhaumik and S. Inagaki, *J. Am. Chem. Soc.*, 2001, **123**, 691.
20 B. Tian, X. Liu, B. Tu, C. Yu, J. Fan, L. Wang, S. Xie, G. D. Stucky and D. Zhao, *Nature Mater.*, 2003, **2**, 159.
21 D. Son, *Appl. Phys. Lett.*, 2004, **85**, 5875.
22 J. S. Pena, P. Soudan, C. O. Arean, G. T. Palomino and S. Franger, *J. Solid State Electrochem.*, 2006, **10**, 1.
23 D. Yu, C. Wu, Y. Kong, N. Xue, X. Guo and W. Ding, *J. Phys. Chem. C*, 2007, **111**, 14394.
24 D. Yang, Z. Lu, X. Rui, X. Huang, H. Li, J. Zhu, W. Zhang, Y. M. Lam, H. H. Hng, H. Zhang and Q. Yan, *Angew. Chem. Int. Ed.*, 2014, **53**, 9352.
25 M. Pramanik, Y. Tsujimoto, V. Malgras, S. X Dou, J. H. Kim and Y. Yamauchi, *Chem. Mater.*, 2015, **27**, 1082.
26 X. Guo, W. Ding, X. Wang and Q. Yan, *Chem. Commun.*, 2001, 709.
27 D. Yu, J. Qian, N. Xue, D. Zhang, C. Wang, X. Guo, W. Ding and Y. Chen, *Langmuir*, 2007, **23**, 382.
28 Q. Yuan, A. X. Yin, C. Luo, L. D. Sun, Y. W. Zhang, W. T. Duan, H. C. Liu and C. H. Yan, *J. Am. Chem. Soc.*, 2008, **130**, 3465.
29 D. Zhao, Q. Huo, J. Feng, B. F. Chmelka and G. D. Stucky, *J. Am. Chem. Soc.*, 1998, **120**, 6024.
30 C. Park, J. Yoon and E. L. Thomas, *Polymer*, 2003, **44**, 6725.
31 S. K. Das, M. K. Bhunia, A. K. Sinha and A. Bhaumik, *ACS Catal.* 2011, **1**, 493.
32 D. Enlow, A. Rawal, M. Kanapathipillai, K. S. Rohr, S. Mallapragada, C.T. Lo, P. Thiyagarajan and M. Akinc, *J. Mater. Chem.*, 2007, **17**, 1570.
33 Lutterotti, L. MAUD version 1.85, 2002, http://www.ing.unitn.it/~maud/.
34 X. Wang, Y. Wang, Q. Tang, Q. Guo, Q. Zhang and H. Wan, J. Catal., 2003, 217, 457.
35 M. Kruk and M. Jaroniec, *Chem. Mater.*, 2001, **13**, 3169
36 W. Yue, A. H. Hill, A. Harrison and W. Zhou, *Chem. Commun.*, 2007, 2518.
37 M. Hu, S. Ishihara and Y. Yamauchi, *Angew. Chem. Int. Ed.*, 2013, **52**, 1235
38 S. Acharya, A. B. Panda, S. Efrima and Y. Golan, *Adv. Mater.*, 2007, **19**, 1105.
39 S. Wu, Z. Zeng, Q. He, Z. Wang, S. J. Wang, Y. Du, Z. Yin, X. Sun, W. Chen and H. Zhang, *Small*, 2012, **8**, 2264.
40 R. Ivanova, B. Lindman and P. Alexandridis, *Langmuir*, 2000, **16**, 9058.
41 P. Alexandridis, R. Ivanova and B. Lindman, *Langmuir*, 2000, **16**, 3676.
42 R. W. Taft and M. J. Kamlet, *J. Am. Chem. Soc.*, 1976, **98**, 2886.
43 Z. Tang, N. A. Kotov and M. Giersig, *Science*, 2002, **297**, 237.
44 S. A. Davis, M. Breulmann, K. H. Rhodes, B. Zhang and S. Mann, *Chem. Mater.*, 2001, **13**, 3218.
45 M. Kanehara, Y. Oumi, T. Sano and T. Teranishi, *J. Am. Chem. Soc.*, 2003, **125**, 8708.
46 X. Y Chen, J. R. Li, L. Jiang, X. Y. Chen and J. R. Li, *Nanotechnology*, 2000, **11**, 108.